

SYSTEM THEORETIC APPROACH TO NMR IMAGING

by

KOMARAVOLU PHANI RAJ KUMAR



DEPARTMENT OF ELECTRICAL ENGINEERING
INDIAN INSTITUTE OF TECHNOLOGY, KANPUR
MARCH 1986

SYSTEM THEORETIC APPROACH TO NMR IMAGING

A Thesis Submitted
In Partial Fulfilment of the Requirements
for the Degree of

MASTER OF TECHNOLOGY

by
KOMARAVOLU PHANI RAJ KUMAR

to the
DEPARTMENT OF ELECTRICAL ENGINEERING
INDIAN INSTITUTE OF TECHNOLOGY, KANPUR
MARCH 1986

107 86

Th
57138111
i j u

11 2 11
CENTRAL LIBRARY
A 91925

EE-1986 N-KUM-SYS

CERTIFICATE

This is to certify that the thesis titled 'System Theoretic Approach to NMR Imaging' submitted by Mr Komaravolu Phani Raj Kumar, Roll No 8410422, in partial fulfilment of the requirements for the award of M Tech degree, has been carried out under our supervision and has not been submitted elsewhere for a degree

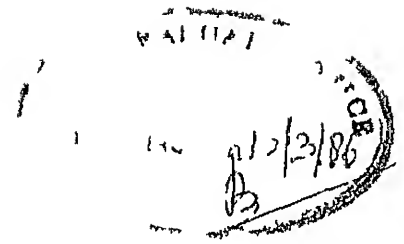
K R Srivathsan

(K R Srivathsan)
Assistant Professor
Department of Electrical Engg
Indian Institute of Technology
Kanpur

K R Sarma

(K R. Sarma)
Professor
Department of Electrical Engg
Indian Institute of Technology
Kanpur

March, 1986



ACKNOWLEDGEMENTS

I express my deep sense of gratitude to Dr K R Sarma for the guidance and encouragement I sincerely thank Dr K R Srivathsan for many useful discussions I had with him

I acknowledge with pleasure the help, in the form of literature and suggestions, provided by Dr Bernhard Blumich, Max-Planck Institut for Polymerforschung, Mainz

I thank Dr P Raghunathan for sailing me through the initial phase of NMR My thanks are due to Dr P T Narasimhan's NMR group for allowing me to have a free access to their literature

Finally, I acknowledge the excellent typing work of Mr C M Abraham

Komaravolu Phani Raj Kumar

ABSTRACT

The work presented in this thesis relates to the signal processing for NMR imaging. The problem of NMR imaging is viewed as a system identification problem. The Bloch equation governing the NMR imaging is treated as state variable representation of the system to be identified. The RF signal excitation is treated as the input and the gradient signals are viewed as system parameters. Thus the NMR imaging system is a linear time varying system, and the identification problem amounts to finding the initial state given the response (FID signal) over an interval of time. The existing modalities of NMR imaging are explained in this point of view.

NMR chirp imaging, based on stochastic imaging is proposed. This scheme of imaging exhibits important merits over other pulse sequences. One is simplicity in generating gradient functions. In NMR imaging the quest for high spatial resolution is of fundamental concern in clinical applications. The proposed chirp imaging permits slow switching of field gradients, admitting stronger gradients for improved resolution. In addition this scheme may permit, using charge coupled device hardware thereby reducing the hardware complexity.

Computer simulation is carried out for obtaining the FID signal for stochastic excitation and chirp imaging. The appropriate signal processing techniques are simulated and the processed images are found to be in close agreement with the assumed models.

CONTENTS

	Page
Chapter 1 INTRODUCTION	1
1 1 Principles of NMR Imaging	1
1 2 Basic NMR Imaging Components	7
1 3 Historical Background	9
1 4 System Theory Approach	10
1 5 Scope of this Thesis	11
Chapter 2 MATHEMATICAL MODEL	12
2 1 Bloch Equation	12
2 2 Excitation Methodologies	14
2 3 Perturbation Analysis	15
Chapter 3 SIGNAL PROCESSING	21
3 1 NMR Detection System	21
3 2 Stochastic NMR Imaging	26
3 3 Chirp Imaging	32
Chapter 4 SIMULATION	37
4 1 Stochastic NMR Imaging Simulation	37
4 1 1 Discretization of the spin density	37
4 1 2 Numerical simulation	39
4 2 Chirp Imaging Simulation	45
4 2 1 1-D Simulation	45
4 2 2 2-D Simulation	48
4 3 Details of Programs	49
Chapter 5 CONCLUSIONS	53
References	55

CHAPTER 1

INTRODUCTION

Nuclear Magnetic Resonance (NMR) is an indispensable tool for material characterization in many disciplines. Recently it has been applied as a method of internal imaging, and in this role NMR enjoys advantages like non-invasive, penetrating bony structure without any attenuation, non hazardous nature, high resolution capability, potential for specific imaging.

In this chapter we discuss the principles of NMR and its applications in imaging context. The hardware associated with NMR imaging system, historical development and system theory approach to NMR imaging is presented. The NMR imaging problem can be viewed as a system identification problem, which is well studied in communication and control area and this view point is elaborated in this thesis.

1.1 PRINCIPLES OF NMR IMAGING [13]

Nuclear Magnetic Resonance is based on the fact that the atomic nuclei of most elements possess a 'spin' which in turn is associated with a small nuclear 'magnetic moment'. The nucleus, e.g., the hydrogen atom or proton, can therefore be imagined as behaving like a tiny bar magnet or compass needle (a magnetic dipole). In the absence of an external magnetic

field the directions of these dipoles have a random orientation (Fig 1 1(a)), but with the application of an external static magnetic field the nuclei begin to precess describing a conical path around the magnetic field direction with a frequency proportional to field strength (Fig 1 1(b)) This frequency is called nuclear magnetic resonance frequency or Larmor frequency. Energy considerations favour orientation of the nuclear dipoles in a direction parallel to the applied field direction and the majority of dipoles precess such that their points tend more towards this direction. The sum of these elementary dipoles results in a macroscopic magnetization (\vec{M}). Applying a radio frequency (RF) pulse brings all the nuclear spins into phase. All the precessing dipoles in phase, produces an alternating magnetic field capable of inducing into a pick-up coil an alternating current of resonating frequency which could be measured. When the RF pulse is removed, detection of the nuclear signal induced into the receiver coil by free precession is then possible. This induced signal is known as a Free Induction Decay (FID) signal.

The resonance phenomenon can be visualized from quantum mechanical description of NMR (Fig 1 2). When proton nuclei are placed in a magnetic field, the nuclei will be in two energy states, namely $+\mu H$ and $-\mu H$ states [7], where μ and H

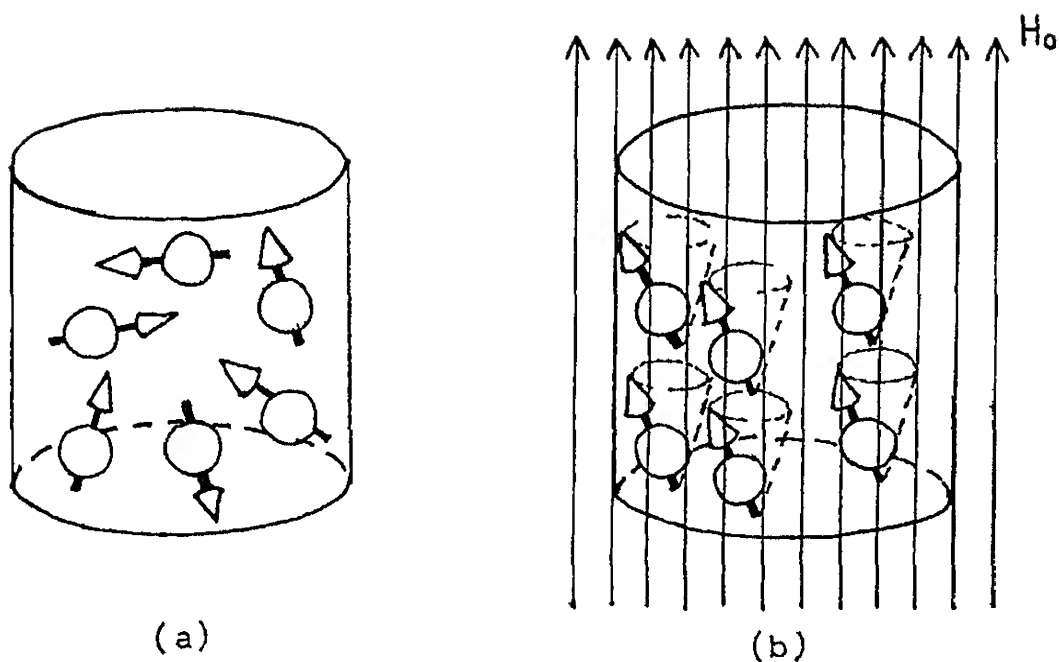


Fig 1 1 Behaviour of nuclear spins (a) without magnetic field
(b) with strong magnetic field

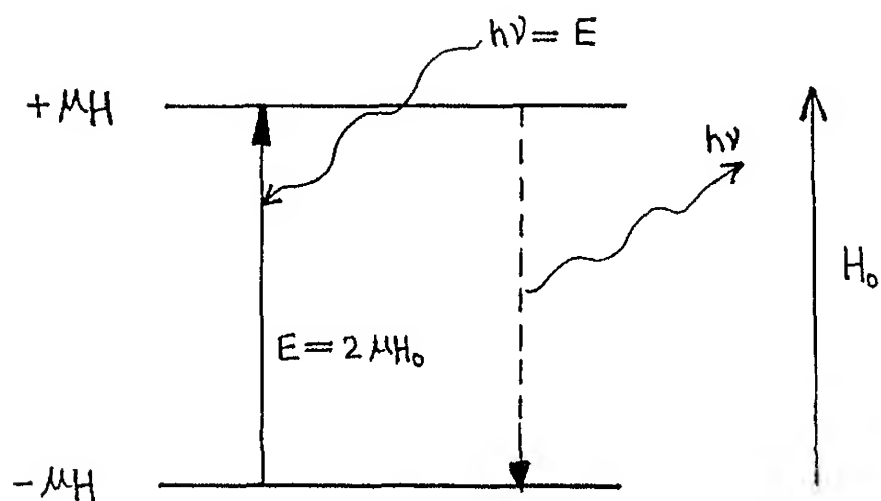


Fig 1 2 Quantum mechanical description of NMR spin excitation

are the nuclear magnetic moment and applied magnetic field, respectively. For those nuclei in $-\mu H$ energy state, irradiation of electromagnetic radiation of energy E equivalent to $2 \mu H$ will raise the proton energy state up to $+\mu H$. This energy is usually supplied by an RF magnetic field.

If an auxiliary magnetic field is applied by means of gradient coils so that, for example, the field of the magnet increases linearly from left to right then the protons at the extreme left of the body will have the lowest nuclear resonance frequency, with the frequency increasing linearly to the right depending on the gradient field, thus the spatial coordinates are mapped to frequency scale. The amplitude of the NMR signal at a particular frequency, hence, is proportional to the number of nuclear spins (e.g., protons) on resonance at the corresponding spatial coordinate.

To obtain information about the structure of more complex three-dimensional form (like human head) having within it an uneven distribution of proton concentrations, magnetic field gradients need to be applied in all directions so that frequency values may be assigned to coordinates throughout the object.

The relaxation mechanisms associated with excited nuclear spins are transverse relaxation (T_2) and longitudinal relaxation (T_1). T_2 is faster than T_1 so that T_2 is always smaller than T_1 .

The characterization of tissue matter is in terms of water content. Water is the medium in which most of the body chemistry or metabolism takes place, hence it plays an essential role in all biological systems [18]. The reason why water has so far played a minor role in medical diagnosis is simply the fact that until the advent of NMR imaging, there really was no way of studying it in vivo. Although NMR imaging will doubtless find applications in the study of plants and fluid transport, emphasis is placed here on the study of biological tissue in man. Biological tissue contains on average around 75% water (Fig 1.3), which can readily be detected by NMR methods. Quite a large fraction of water is contained within the cell cytoplasm but there is also a substantial amount of extra cellular water in addition to the bulk fluids contained within the body. Different healthy body tissues contain different amounts of water and variations in water content can be used to some extent to differentiate the various human tissues although the variations between tissues are rather small.

It is also found experimentally that there are differences in the spin relaxation times of various tissues and there is a good correlation between the spin-lattice relaxation time T_1 and water content among the various animal tissues, the longer T_1 's being observed in tissues with higher water content. Damadian [8] has shown that T_1 is longer in malignant tissue

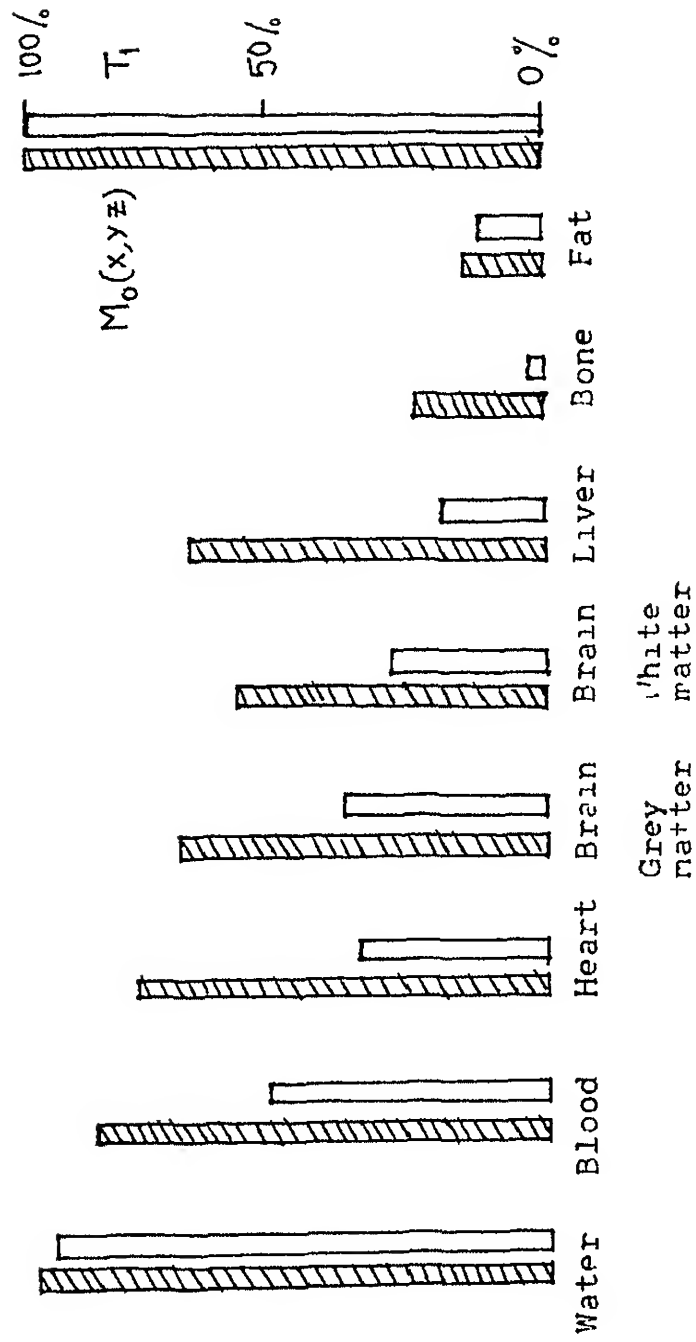


Fig 1.3 Water content, relaxation time in various human tissues

by a factor of about 1.5 to 2.0. Such pathological tissue is also found to contain more water. It would thus seem from the tissue characteristics that an imaging method based on water content and/or T_1 would easily differentiate between the various tissue types yielding cross-sectional images showing anatomical detail as reflected in the distribution of water throughout the body. The spin-spin relaxation time T_2 , which also varies with tissue type, might be similarly used, given suitable modification of the imaging method. Imaging capabilities of these two important parameters, T_1 and T_2 , together with the spin densities make NMR imaging a unique, versatile, and powerful technique in medical imaging.

1.2 BASIC NMR IMAGING COMPONENTS [11]

A typical NMR imaging system designed for human imaging is shown in Fig. 1.4 [7]. The basic components of an NMR imaging are as follows:

- 1) A magnet, which provides a strong (range - 500 G to 15 KG), uniform, static magnetic field (H_0)
- 2) An RF transmitter, which delivers radio frequency (range - 2 to 70 MHz for proton imaging) magnetic fields to the sample ($H_1(t)$)
- 3) A gradient system, which produces time varying magnetic fields (range - 0.01 to 1 G/cm) of controlled spatial nonuniformity ($G_x(t)$, $G_y(t)$, $G_z(t)$)

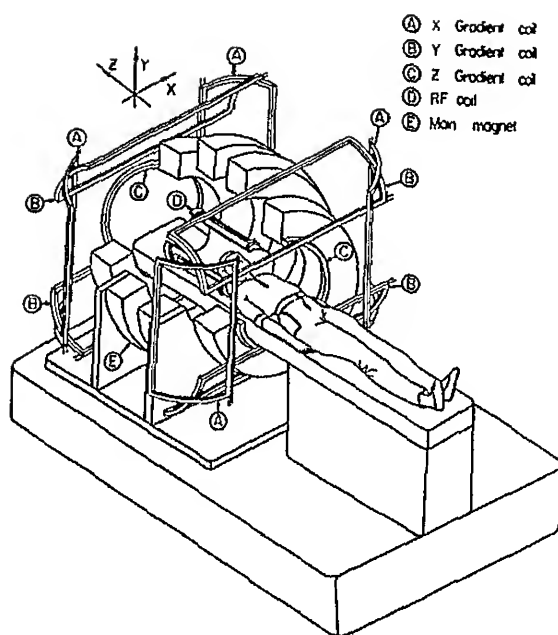


Fig 1.4 Sketch of NMR tomograph [7]

- 4) A detection system, which yields the output signal $(y(t))$
- 5) An imager system, which reconstructs and displays the images

Imaging system shown in Fig 1.4 uses a single RF coil which is used for both transmission of RF signal (longest RF pulse duration is on the order of 2 ms) and reception of FID signal (like a Pulsed Radar) The stochastic imaging discussed in the next section assumes two coils one for transmission and other for reception, since transmission and reception are done simultaneously

Resolution in a conventional NMR imaging system depends on the field homogeneity and available strength of field gradients For example, with a magnet of the static magnetic field of $H_0 = 5 \text{ KG}$ having homogeneity of $\Delta H = 4 \text{ ppm}$ (0.02 G) with field gradient of $G_{x,y \text{ or } z} = 0.4 \text{ G/cm}$, the expected resolution limit is approximately 0.5 mm The physical arrangement of components and instrumentation is an important factor in NMR tomography

1.3 HISTORICAL BACKGROUND [18]

At the beginning of 1970's both Lauterbur [16] and Damadian [8] showed that NMR spectroscopic techniques can be applied to imaging of the human body and that the techniques have diagnostic uses similar to those of X-ray computerized

tomography (CT) In 1978, Andrew et al demonstrated the very-high-resolution capability of NMR by obtaining a fine detail image of the submillimeter septum of a small orange. More recently, human head images shown by Moore and Holland et al have definitely demonstrated the great potential of NMR imaging in medical imaging. Already the subject has acquired a variety of names of which more common are NMR imaging, spin mapping, Zeugmatography, NMR tomography.

1.4 SYSTEM THEORY APPROACH

It is well known that a linear time invariant (LTI) system is completely characterized by its impulse response. System identification problem is equivalent to the impulse response determination. Various methods used in impulse response determination of LTI systems can be broadly classified as sinusoidal wave testing, pulse testing and cross correlation method. These are the familiar techniques already in usage in NMR. In correlation method an input signal with impulsive autocorrelation function is applied to the system and the response is crosscorrelated with shifted versions of input signal to obtain impulse response point by point.

In case of linear time varying (LTV) systems, response of the system for an arbitrary input cannot be given in a closed form as in the case of LTI systems. But in general when infinite series solution is obtained under conditions which permit

the system to be viewed as under perturbation, the solution resembles that of a LTI system. In NMR imaging equations governing the system behaviour (Bloch equation) correspond to that of LTV system under the conditions, the input RF excitation is small [12] the response resembles the familiar convolution integral and hence amenable to cross correlation approach. The output of cross correlation operation gives the information regarding the spatial spin distribution [2]. Details of this approach are given in Chapter 2.

1.5 SCOPE OF THIS THESIS

Chapter 2 develops the mathematical model of NMR imaging problem, NMR imaging is treated in the system theoretic point of view as LTV system, described by state representation. Solution of the state equations is discussed. Chapter 3 covers the cross correlation techniques to process the FID signal to obtain the spatial spin distribution. Chapter 4 discusses the computer simulation of NMR imaging system model and the signal processing schemes. FID signal corresponding to specified gradients and RF excitation are generated by computer using the model. Associated cross correlation scheme is applied to obtain the assumed spin distribution. Chapter 5 concludes the thesis with suggestions for future work.

CHAPTER 2

MATHEMATICAL MODEL

2.1 BLOCH EQUATION

The Bloch equation [1], gives an accurate but phenomenological description of the time dependence of the 'nuclear magnetization' $M(t)$ in the presence of an applied magnetic field $H(t)$. The nuclear magnetization $M(t)$ is the source of the 'NMR Signal' from which the image is ultimately constructed. The NMR sample is treated as a black box with $H(t)$ as the input signal, or stimulus, and $M(t)$ as the output signal or response. The black box is characterized by $M_0(x, y, z)$, T_1 and T_2 , and its behaviour by the Bloch equation

$$\frac{d\vec{M}}{dt} = \gamma \vec{M} \times \vec{H} - \left(\frac{M_x u_x + M_y u_y}{T_2} \right) - \left(\frac{M_z - M_0}{T_1} \right) u_z \quad (2.1)$$

The above equation can be conveniently represented in matrix notation as

$$\begin{bmatrix} \dot{M}_x \\ \dot{M}_y \\ \dot{M}_z \end{bmatrix} = \begin{bmatrix} -\frac{1}{T_2} & \gamma h & 0 \\ -\gamma h & -\frac{1}{T_2} & \gamma H_1(t) \\ 0 & -\gamma H_1(t) & 0 \end{bmatrix} \begin{bmatrix} M_x \\ M_y \\ M_z \end{bmatrix}$$

List of Symbols

$\overline{\int}$	Three dimension Integral
Im	Imaginary part of
Re	Real part of
H_0	Strength of the static magnetic field
γ	Gyromagnetic ratio For protons its value is $4.26 \times 10^7 \text{ Hz Tesla}^{-1}$
$h(t, x, y, z)$	Gradient magnetic field $(G_x(t)x + G_y(t)y + G_z(t)z) u_z$ Its effect in u_x, u_y is neglected because u_z term dominates
$H(t, x, y, z)$	Total magnetic field experienced at t, x, y, z (represented as \vec{H} or $H(t)$) It has components in u_x, u_y and u_z directions
$H_1(t)$	Input RF signal Its effect is only u_x direction
$M(t, x, y, z)$	Sample magnetization at t, x, y, z (represented as \vec{M} or $M(t)$)
M_x, M_y, M_z	Components of \vec{M}
$M = M_x + jM_y$	(Complex) transverse magnetization
$M_0(x, y, z)$	Equilibrium magnetization or spin density
$\omega_0 = -\gamma H_0$	Larmour frequency corresponding to the static field
ω	Irradiation frequency of the RF field
u_x, u_y, u_z	Unit vectors in x, y, z directions respectively
$G_x(t), G_y(t), G_z(t)$	Gradient magnetic fields applied along x, y, z axes respectively

The nuclear magnetization $\vec{M}(t)$, induced in the sample by the magnetic field $H(t)$, is the local sum of the magnetic fields of the protons. The magnetization is a bulk property of the sample rather than that of individual protons.

2.2 EXCITATION METHODOLOGIES

Two kinds of excitations are seen in NMR imaging. First, short-pulse excitation in which first a RF pulse, sufficient to tilt magnetization into transverse plane, is applied. At the end of RF pulse, field gradients are applied during which FID signal is recorded. Second, both excitation and gradients are applied simultaneously throughout the experiment and FID signal is recorded.

Short Pulse excitation method can be conveniently explained through the Bloch equation discussed earlier. The system dynamics after the application of excitation pulse is given by

$$\begin{bmatrix} M_x \\ M_y \\ M_z \end{bmatrix} = \begin{bmatrix} -\frac{1}{T_2} & \gamma h & 0 \\ -\gamma h & -\frac{1}{T_2} & 0 \\ 0 & 0 & 0 \end{bmatrix} \begin{bmatrix} M_x \\ M_y \\ M_z \end{bmatrix}$$

and initial conditions change from

$$\begin{bmatrix} 0 \\ 0 \\ M_0(x, y, z) \end{bmatrix}$$

to

$$\begin{bmatrix} M_{x_0}(x,y,z) \\ M_{y_0}(x,y,z) \\ 0 \end{bmatrix}$$

where $M_0(x,y,z) = \sqrt{M_{x_0}(x,y,z)^2 + M_{y_0}(x,y,z)^2}$ Solution for
M can be given as

$$M = e^{-t/T_2} e^{-j\gamma \int_0^t h(t') dt'} M_{xy_0}(x,y,z)$$

where $M_{xy_0}(x,y,z) = M_{x_0}(x,y,z) = -jM_{y_0}(x,y,z)$

It is interesting to note that similar solution is arrived at
in stochastic NMR imaging

2 3 PERTURBATION ANALYSIS [12]

In this method both input excitation and gradients are
considered at same time

Equation (2 1) can be written as

$$\frac{dM_x}{dt} = -\frac{M_x}{T_2} + M_y \gamma h \quad (2 2)$$

$$\frac{dM_y}{dt} = -M_x \gamma h - \frac{M_y}{T_2} + M_z \gamma H_1(t) \quad (2 3)$$

$$\frac{dM_z}{dt} = -M_y \gamma H_1(t) - \left(\frac{M_z - M_0}{T_1} \right) \quad (2 4)$$

Let $M = M_x + jM_y$

The equations (2 2), (2 3) and (2 4) may be written, neglecting spin-lattice relaxation (i.e., $t \ll T_1$) in the form

$$\frac{dM}{dt} + \left(\frac{1}{T_2} + j\gamma h\right)M = j\gamma H_1(t) M_z \quad (2 5)$$

$$\frac{dM_z}{dt} = -\gamma H_1(t) \text{Im } M \quad (2 6)$$

Due to linear time varying characteristics of a driven NMR system it is usual to discard the simple methods of Fourier analysis applicable to other spectroscopic forms. The particular case considered here is the response of the NMR system to an arbitrary shaped pulse of duration less than T_2 . The approach to be employed is a combination of perturbation theory and linear system analysis [19]

Let us recall that M is a complex quantity, $M_x + jM_y$, and M_z real. These can be expanded as

$$M = M^{(0)} + M^{(1)} + M^{(2)} + M^{(3)} + \dots \quad (2 7)$$

$$M_z = M_z^{(0)} + M_z^{(1)} + M_z^{(2)} + \dots \quad (2 8)$$

$M^{(n)}$ and $M_z^{(n)}$ are small quantities of the n th order. Assuming that the driving function $H_1(t)$ represents but a small perturbation to the Hamiltonian of the NMR system, i.e., applied excitation amplitude is far less than the static magnetic field, and that $M^{(n)}$ and $M_z^{(n)}$ are zero when $H_1(t) = 0$. Substituting eq.

(2 7) in (2 5) and (2 8) in (2 6) yields a set of equations of various orders, and representative equations of one order are

$$\frac{dM^{(n)}}{dt} + \left(\frac{1}{T_2} + j\gamma h\right) M^{(n)} = j\gamma H_1(t) M_z^{(n-1)} \quad (2 9)$$

$$\frac{dM_z^{(n)}}{dt} \approx -\gamma H_1(t) \operatorname{Im} M^{(n-1)} \quad (2 10)$$

Thus, $M^{(n)}$ may be calculated in terms of $M_z^{(n-1)}$, $M_z^{(n-1)}$ in terms of $M^{(n-2)}$ and so on. In other words, knowing the lowest-order terms, all other terms may, in principle be calculated from these recurrence relationships. Quantities such as $\gamma H_1(t) M_z^{(n-1)}$ are of order n as $H_1(t)$ is small. Consider first the zeroth-order terms

$$\frac{dM^{(0)}}{dt} + \left(\frac{1}{T_2} + j\gamma h\right) M^{(0)} = 0 \quad (2 11)$$

However, in the absence of any irradiation, we know that M must be zero and so $M^{(0)} = 0$ (No tilting of magnetization vector into transverse plane and hence no reading in that plane). The equation in M_z gives

$$\frac{dM_z^{(0)}}{dt} \approx 0, \quad (2 12)$$

and so $M_z^{(0)}$ is constant which may equate with the equilibrium magnetization $M_0(x, y, z)$. Moving on to the first-order equations

$$\frac{dM_z^{(1)}}{dt} + \left(\frac{1}{T_2} + j\gamma h\right) M_z^{(1)} = j\gamma H_1(t) M_z^{(0)} = j\gamma H_1(t) M_0(x, y, z) \quad (2.13)$$

This equation will be analyzed in considerable detail later

Also,

$$\frac{dM_z^{(1)}}{dt} \approx -\gamma H_1(t) M_z^{(0)} = 0$$

This is a repeat of eq (2.12), but as $M_z^{(1)}$ is zero for $H_1(t) = 0$, it must be zero all times

$$\begin{aligned} M_z &= M_z^{(0)} + M_z^{(1)} + \dots \\ &= M_0 + 0 + \dots \end{aligned}$$

The second-order equations thus give

$$\frac{dM_z^{(2)}}{dt} + \left(\frac{1}{T_2} + j\gamma h\right) M_z^{(2)} = 0 \quad (M_z^{(1)} = 0)$$

and here $M_z^{(2)}$ is zero for the same reasons

$$\frac{dM_z^{(2)}}{dt} \approx -\gamma H_1(t) \text{Im } M_y^{(1)}$$

Hence

$$M_z^{(2)} \approx \int_{-\infty}^t -\gamma H_1(t) M_y^{(1)} dt$$

This term describes the departure of the magnetization from the equilibrium alignment along the z-axis. Finally, the third order equation in M is

$$\frac{dM^{(3)}}{dt} + \left(\frac{1}{T_2} + j\gamma h\right) M^{(3)} = j\gamma H_1(t) M_z^{(2)}$$

and this expression describes the deviation of M from the linear behaviour of Eq (2 13)

Equation (2 13) describes a linear differential equation, and so the technique of linear systems analysis may be brought to bear on the problem of solving the equation [19] Hence,

$$M^{(1)} = e^{-\int_0^t \left(\frac{1}{T_2} + j\gamma h\right) dt'} \int_0^t j\gamma H_1(t_1) M_0(x, y, z) e^{\int_0^{t_1} \left(\frac{1}{T_2} + j\gamma h\right) dt'} dt_1 \quad (2 14)$$

writing Eq (2 14) in detail we have

$$M^{(1)} = \exp \left[-\int_0^t \frac{1}{T_2} + j\gamma H_0 + j\gamma x G_x(t') + j\gamma y G_y(t') + j\gamma z G_z(t') dt' \right] \int_0^t j\gamma H_1(t_1) M_0(x, y, z) \exp \left[\int_0^{t_1} \frac{1}{T_2} + j\gamma H_0 + j\gamma x G_x(t') + j\gamma y G_y(t') + j\gamma z G_z(t') dt' \right] dt_1 \quad (2 15)$$

Substitution of $t_1 - t = \tau$ yields

$$M^{(1)} = -j\gamma M_0(x, y, z) \int_0^t H_1(t - \tau) e^{-\tau \left(\frac{1}{T_2} + j\gamma H_0\right)} e^{j\gamma x \int_t^{t-\tau} G_x(t') dt'} e^{j\gamma y \int_t^{t-\tau} G_y(t') dt'} e^{j\gamma z \int_t^{t-\tau} G_z(t') dt'} d\tau \quad (2 16)$$

With (2 1b) as the base, solution for remaining terms can be written, at least in principle. Hoult [12] showed in computer simulation studies that under the assumption that when input excitation is small enough to tilt magnetization vector from static field alignment by an angle less than 30° the effect of $M^{(3)}$ and higher order terms can be neglected and the dominant term is only $M^{(1)}$. Our further analysis takes only $M^{(1)}$ term into consideration.

Hence, receiver coil output is spatial integral of $M^{(1)}$ term only and estimation of spatial information (spin density) on this output is a fair approximation.

Similar solution (Eq (2 16)) can be arrived at using Kinariwala's approach [10]. This approach is to decompose the square matrix represented under Eq (2 1) into two matrices, $A_0(t)$ and $A_1(t)$, where $A_0(t)$ satisfies the commutative condition $A_1(t)$ is interpreted as a perturbation upon $A_0(t)$. This method is very similar to Hoult's perturbation analysis, except whole matrix is considered instead of individual terms.

CHAPTER 3

SIGNAL PROCESSING

3.1 NMR DETECTION SYSTEM

Expression for $\bar{M}(t)$, the nuclear magnetization is derived in the previous chapter. It is the function of the NMR detection system, the receiver, to detect $\bar{M}(t)$ and generate an output signal $y(t)$. The receiver coil, which usually surrounds the sample, is an antenna which picks up the fluctuating nuclear magnetization of the sample and converts it to a fluctuating output voltage $V(t)$, where

$$V(t) = - \frac{d}{dt} \int \bar{M}(t, \bar{x}) \cdot B_c(\bar{x}) d\bar{x}$$

The function $B_c(\bar{x})$ describes the sensitivity of the receiver coil at different points in space. The primary objective of receiver coil design is to prescribe wire placements so that $B_c(\bar{x})$ has the largest possible transverse component. The longitudinal component of $B_c(\bar{x})$ contributes little to the output voltage, and can be ignored. This is a result of the fact that the time derivative of $M_z(t, \bar{x})$ is much less than that of transverse component. $M_z(t, \bar{x})$ decays exponentially with the time constant T_1 typically 0.1 to 1 S, while the transverse component is oscillatory with a period of typically, 0.05 to 0.2 μ s. Let

$$B_c(\bar{x}) = au_x + bu_y$$

where a and b are fixed, but unknown constants

Instead of $V(t)$, time integral of $V(t)$ (let this be $y'(t)$) is considered which leads to mathematical simplicity Hence

$$\begin{aligned} y'(t) &= \bar{\int} (aM_x(t, \bar{x}) + bM_y(t, \bar{x})) d\bar{x} \\ &= \bar{\int} \operatorname{Re}((a - jb) M(t, \bar{x})) d\bar{x} \end{aligned}$$

Making the replacements $a = K \cos \phi'$ and $b = -K \sin \phi'$

$$\begin{aligned} y'(t) &= - \bar{\int} \operatorname{Re} K e^{j\phi} M(t, \bar{x}) d\bar{x} \\ &= - \bar{\int} \operatorname{Re} K M(t, \bar{x}) d\bar{x} \end{aligned}$$

where K is complex arbitrary constant

Dropping the constant part we have $\bar{\int} M(t, \bar{x}) d\bar{x}$, and let this be represented by $y''(t)$ In detail $y''(t)$ can be written from Eq (2.16) as

$$\begin{aligned} y''(t) &= \iiint M_0(x, y, z) \int_0^t H_1(t-\tau) e^{-\tau(\frac{1}{T_2} + j\gamma H_0)} \\ &\quad e^{j\gamma x} \int_t^{t-\tau} G_x(t') dt' \quad e^{j\gamma y} \int_t^{t-\tau} G_y(t') dt' \\ &\quad e^{j\gamma z} \int_t^{t-\tau} G_z(t') dt' d\tau dx dy dz \end{aligned}$$

By quadrature phase detection $j\gamma H_0$ term can be eliminated

Let $y''(t)$ after quadrature phase detection be represented as $y(t)$ With the definitions

$$u(t, \tau) = \gamma \int_t^{t-\tau} G_x(t') dt'$$

$$v(t, \tau) = \gamma \int_t^{t-\tau} G_y(t') dt'$$

and

$$w(t, \tau) = \gamma \int_t^{t-\tau} G_z(t') dt'$$

$y(t)$ can be written as

$$y(t) = \int_{-\infty}^{+\infty} \int_{-\infty}^{\infty} \int_{-\infty}^{\infty} M_0(x, y, z) \int_0^t H_1(t-\tau) e^{-\tau/T_2} e^{jxu(t, \tau)} e^{jyv(t, \tau)} e^{jzw(t, \tau)} d\tau dx dy dz \quad (3.1)$$

The imaging experiment is treated in terms of system analysis. The underlying concept is that of a black box which is tested with an input signal $H_1(t)$ and responds with an output signal $y(t)$. The feature to be revealed in this imaging experiment is the spin density distribution of the biological sample as a function of space coordinates. For T_1 and T_2 imaging a different methodology has to be adopted. From Eq (3.1) it can be seen that four variables (shape of the RF input signal, and the modulations of magnetic x, y, z gradients) are at our disposal. Consequently the imaging experiment may be treated as a four-input time invariant system or a one-input, time dependent system, when the time dependence is imposed by the magnetic field gradients and the one input is the RF signal. More specifically, the NMR imaging experiment is described in terms of a linear time-dependent system.

Broadly imaging modalities may be classified as being 'reconstructive' or 'non-reconstructive'. The former technique is an adaptation of the principles of image generation in X-ray CT, and involves reconstruction of the image in its entirety from integral projections.

Modalities in which an image reconstruction scheme is not involved are classified as non-reconstructive. These can be classified in two different ways.

- (i) Based on dimension 1-Dimension, 2-Dimension, 3-Dimension
Using appropriate excitation signal and gradients, it is possible to excite desired section in spin density volume (Fig 4.5)
- (ii) Based on pulse sequence ^e Varieties of pulse sequences are in usage. A specific method known as Kumar, Wclti, and Ernst (KWE) direct Fourier NMR tomographic imaging is discussed below.

The RF pulse and gradient sequence used in KWE method is illustrated in Fig. 3.1 and commences at $t = 0$ with a short nonselective RF pulse to nutate some or all of the equilibrium magnetization into the x, y plane. This is then followed by periods t_x and t_y of variable length during which linear magnetic field gradients G_x, G_y are applied in x and y directions respectively. Finally, the FID is sampled in the presence of a z -gradient G_z for a time $t_z = t - (t_x + t_y)$.

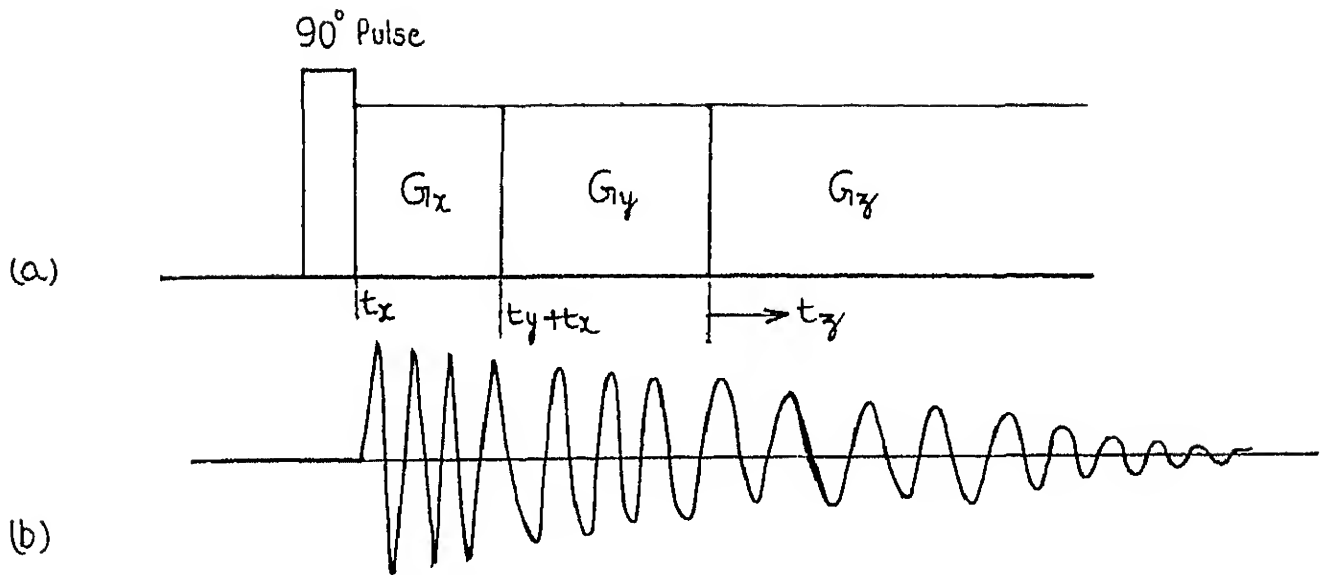


Fig. 3.1 (a) Pulse sequence used in k-f imaging method
(b) FID signal

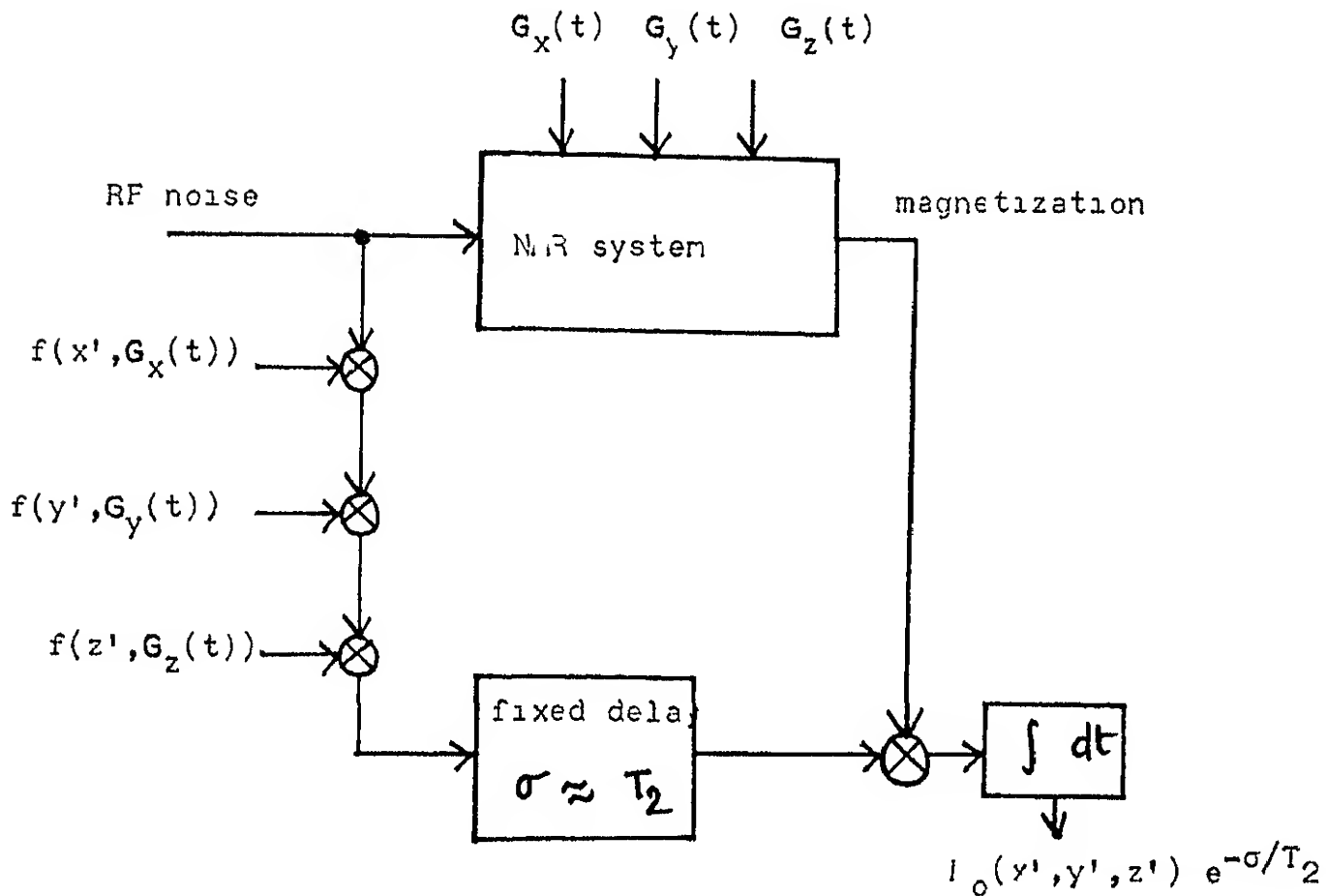


Fig. 3.2 Cross correlation scheme in NMR imaging

The z component of the magnetic field is therefore given by

$$\begin{aligned} H_0 + G_x x & \quad 0 < t < t_x \\ H_0 + G_y y & \quad t_x < t < t_x + t_y \\ H_0 + G_z z & \quad t_x + t_y < t \end{aligned}$$

and the response of the spin system $y(t)$ will be a function of t_x and t_y , as well as t_z , i.e., $y(\vec{t}) = y(t_x, t_y, t_z)$. The experiment is repeated for a full set of regularly stepped or incremented t_x and t_y values allowing a three-dimensional image of the object to be reconstructed as discussed below.

The observed signal $y(\vec{t})$ can be written from Eq. (3.1) as

$$y(\vec{t}) = \iiint M_0(x, y, z) e^{j\gamma G_x x t_x} e^{j\gamma G_y y t_y} e^{j\gamma G_z z t_z} e^{-(t_x + t_y + t_z)/T_2} dx dy dz$$

Neglecting the effect of T_2 , $M_0(x, y, z)$ can be obtained by inverse 3-D Fourier transform as given below

$$M_0(x', y', z') = \iiint y(t_x, t_y, t_z) e^{-j\gamma G_x x' t_x} e^{-j\gamma G_y y' t_y} e^{-j\gamma G_z z' t_z} dt_x dt_y dt_z$$

3.2 STOCHASTIC NMR IMAGING [2]

Stochastic excitation denotes a noise-modulated RF input signal, which is supplied for the entire length of the imaging experiment. RF noise is conveniently generated by a sequence of RF pulses with random flip angles. The pulses are separated by

the sampling interval Δt . For each input pulse one value of the response is sampled. The stochastic RF excitation delivers its excitation energy to the NMR system within a characteristic relaxation time T_1 . While pulsed excitation concentrates the same energy into a single pulse of length Δt .

The spin density is retrieved from cross correlation of input and output records. The longer these records, the better will be achievable signal to noise ratio (SNR) of the spin density. In stochastic system analysis the input signal usually is white noise with zero mean so that the autocorrelation of the real-valued input is proportional to a delta function

$$\lim_{T \rightarrow \infty} \frac{1}{T} \int_0^T H_1(t) H_1(t-\sigma) dt = \mu_2(\sigma) \quad (3.2)$$

The proportionality constant μ_2 is the second moment of the power of the input

For time-invariant systems the linear impulse response function can be retrieved from cross-correlation of input and output signals according to

$$\lim_{T \rightarrow \infty} \frac{1}{T} \int_0^T y(t) H_1(t-\sigma) dt = \mu_2 M'(\sigma) \quad (3.3)$$

where $M'(t)$ is impulse response,

$$M'(t) = \int \bar{M}_0(\bar{x}) \exp \left[-\frac{t}{T_2} + j\gamma \bar{x} \int_0^t G_x(t') dt' \right] d\bar{x},$$

with $M'(t < 0) = 0$. The cross-correlation is a time average of the product of the system response with the delayed input signal. The result is the linear impulse response as a function of the delay σ . In case of time-dependent systems this concept cannot be applied. However, for the imaging system the goal is to retrieve its time-invariant part but not the complete time dependent impulse response. Since the time dependent part is known, the system response $y(t)$ can be correlated with the product of all the time-dependent factors in the response integral

$$P(t-\sigma) = e^{-jx' u(t,\sigma)} e^{-jy' v(t,-\sigma)} e^{-jz' w(t,\sigma)} H_1(t-\sigma) \quad (3.4)$$

The primed coordinates as well as σ become variables in the cross-correlation. Its evaluation yields the spin density as a function of the cross-correlation variables. The complete scheme is shown in Fig. 3.2 [3]

$$\begin{aligned} & \lim_{T \rightarrow \infty} \frac{1}{T} \int_0^T y(t) P(t-\sigma) dt \\ &= \iiint M_0(x, y, z) \int_0^\infty e^{-\tau/T_2} \lim_{T \rightarrow \infty} \frac{1}{T} \int_0^T e^{jxu(t,\tau)} \\ & \quad e^{-jx'u(t,\sigma)} e^{jyv(t,\tau)} e^{-jy'v(t,\sigma)} e^{-jz'w(t,\sigma)} \\ & \quad e^{jzw(t,\tau)} \\ & \quad H_1(t-\tau) H_1(t-\sigma) dt d\tau dx dy dz \end{aligned} \quad (3.5)$$

$$= (2\pi)^3 \mu_2 \iiint M_0(x, y, z) \int_0^\infty e^{-\tau/T_2} \delta(x-x') \delta(y-y') \delta(z-z') \delta(\tau-\sigma) d\tau dx dy dz \quad (3.6)$$

$$= (2\pi)^3 \mu_2 M_0(x', y', z') e^{-\sigma/T_2} \quad (3.7)$$

In Eq (3.5) the cross-correlation has been written down explicitly but the order of integration has been changed. The step from (3.5) to (3.6) involves the evaluation of the inner most integral. The fourfold product of delta functions result from Eq (3.2), the definition of the delta function

$$\frac{1}{2\pi} \int_{-\infty}^{\infty} e^{jk(x-x_0)} = \delta(x-x_0) \quad (3.8)$$

and a postulated orthogonality of the four functions in the product of Eq (3.4). The step from Eqs (3.6) to (3.7) is the evaluation of the delta functions

For the orthogonality to be satisfied three conditions must be met

Condition 1

The input signal $H_1(t)$ must have zero mean

$$\mu_1 = \lim_{T \rightarrow \infty} \frac{1}{T} \int_0^T H_1(t) dt = 0 \quad (3.9)$$

Condition 2

The time integrals over the magnetic field gradients must always be different from zero

$$u(t, \tau), v(t, \tau), w(t, \tau) \neq 0 \quad (3.10)$$

for all t and some given σ

Condition 3

The difference of the local phase angles in the different directions x, y, z should never vanish for all primed and unprimed values of x, y and z

$$\begin{aligned} xu(t, \sigma) - yv(t, \sigma) &\neq 0, \\ yv(t, \sigma) - zw(t, \sigma) &\neq 0, \\ zw(t, \sigma) - xu(t, \sigma) &\neq 0, \end{aligned} \quad (3.11)$$

for all times t , the σ given, and all x, y, z

Condition 1 is trivial. Condition 2 can be fulfilled by modulating a field gradient such that no gradient component ever changes sign. The last condition is the most restricting one. One way to observe it is by using significantly different field gradient in each direction x, y and z . A different gradient scheme is simulated in next chapter for the case where the spin density shall be recovered at discrete coordinates x', y' , and z' .

The final result of the cross correlation (3.7) is the spin density as a function of space coordinates, scaled by the input power, μ_2 , and a negative exponential involving the transverse relaxation time T_2 and the cross-correlation delay σ . Input power μ_2 cannot be made arbitrarily large in order to increase the system response, since eventually the system will become nonlinear and the response will be damped. However, there exists an input power level which yields a response maximum and consequently optimum SNR in the acquisition of the response.

In comparison with pulsed FT NMR, stochastic resonance [4]

- 1) has the same sensitivity ,
- 2) allows an independent optimization of sensitivity and resolution in contrast to pulse FT NMR ;
- 3) reduces the problems in the receiving electronics associated with the large dynamic range of impulse signals,
- 4) reduces the peak excitation power such that wider dynamic ranges may be covered ,
- 5) admits coherent averaging of the system response in connection with cyclic excitation ,
- 6) will exhibit different saturation features. In particular, the nonlinear response will involve double resonance effects;
- 7) investigates the spin system in dynamic equilibrium with the excitation and not the unperturbed thermodynamic equilibrium state

Stochastic excitation in NMR imaging has three advantages over conventional methods with sparsely pulse PF input

- 1) The excitation power is reduced by several orders of magnitude
- 2) Since no deterministic pulse cycle exists, every additionally acquired data point increases the quality of the entire image
- 3) For slowly moving objects, reconstruction of the image can be restricted to those data, during the acquisition of which the object was in approximately the same state

3 3 CHIRP IMAGING

In NMR imaging the quest for high spatial resolution is of fundamental concern in clinical applications. High resolution necessitates the use of strong magnetic field gradients. Conventional imaging schemes traditionally employ fast switching of gradients. Since the speed of switching imposes an upper limit on the usable gradient strength, it is desirable to search for imaging schemes which permit slow switching of field gradients admitting stronger gradients for improved resolution. NMR imaging with sinusoidal field gradient modulation [5],[9] seems to be an attractive solution.

In general an infinite number of gradient modulation functions ($G_x(t, \tau)$, $G_y(t, \tau)$, $G_z(t, \tau)$) are conceivable, which obey the three conditions, Eqs (3 9), (3 10) and (3 11). We

propose a new class of imaging scheme, viz , Chirp processing because of its simplicity in generating gradient functions and subsequent processing structure Chirp processing has been developed to provide a solution for the conflicting requirements of simultaneous long-range and high -resolution performance in radar systems [14] Chirp processing is often interpreted as an alternative to Fourier transform in signal processing

Consider Eq (3 1) After the application of $\pi/2$ pulse, $y(t)$ can be written as

$$y(t) = \iiint M_0(x,y,z) e^{-t/T_2} e^{jxu(t)} e^{jyv(t)} e^{jzw(t)} dx dy dz \quad (3.12)$$

T_2 is a spatial function and hence cannot be brought outside the integral, but let us neglect the effect of T_2

Let the gradients be linear functions of time as given below

$$G_x(t) = K_1 t \quad (3.13)$$

$$G_y(t) = K_2 t \quad (3.14)$$

$$G_z(t) = K_3 t \quad (3.15)$$

and

$$u(t) = \int_0^t K_1 t' dt' = \frac{K_1 t^2}{2} \quad (3.16)$$

$$\text{Similarly} \quad v(t) = \frac{K_2 t^2}{2} \quad (3.17)$$

$$w(t) = \frac{K_3 t^2}{2} \quad (3.18)$$

where K_1, K_2 and K_3 are constants. The three conditions Eqs (3.9), (3.10) and (3.11) are satisfied by this particular choice as per the constraints given below

- 1) Input signal $H_1(t)$ must have zero mean

$$\int_0^{T_P} \sin \omega t \, dt = 0$$

- 2) The time integrals over the magnetic field gradients must always be different from zero

Our choice of field gradients, which are linear functions of time satisfy this property (Eq (3.13), (3.14) and (3.15))

- 3) The difference of the local phase angles in different directions x, y, z should never vanish for all primed and unprimed values of x, y and z . From Eq (3.11)

$$x u(t) - y v(t) \neq 0$$

$$\Rightarrow x K_1 \neq y K_2$$

This is possible to maintain except for some set of values of x, K_1, y, K_2 . All points in x - y plane can be imaged except those lying on straight line $y = x K_1 / K_2$. This problem can be

overcome by repeating the experiment with different Chirp rates, i.e., K_1' and K_2' instead of K_1 and K_2 such that $K_1'/K_2' \neq K_1/K_2$

The constraints under this condition can be given as

$$xK_1 \neq yK_2 \neq zK_3$$

$$\text{and } x'K_1 \neq y'K_2 \neq z'K_3$$

Multiplying $y'(t)$ (Eq (3.12)) with $e^{-jx'K_1 t^2/2} e^{-jy'K_2 t^2/2} e^{-jz'K_3 t^2/2}$ and integrating with respect to time amounts to

$$\iiint M_0(x, y, z) \int e^{jK_1(x-x')t^2/2} e^{jK_2(y-y')t^2/2} e^{jK_3(z-z')t^2/2} dt dx dy dz$$

In the inner integral each term behaves approximately like a delta function

Consider $\delta(x-x') = \int_0^\infty e^{jK_1(x-x')t^2/2} dt$ This can be written as

$$\int e^{-t^2/2\sigma^2}$$

$$\text{where } \sigma = \frac{1}{\sqrt{K_1(x-x')}} \frac{1}{e^{j\pi/4}}$$

From the knowledge of Gaussian function this integral can be written as

$$\sqrt{\frac{\pi}{2}} \frac{1}{\sqrt{K_1}} \frac{1}{\sqrt{x-x'}} \quad , \text{ neglecting the phase part}$$

The above function behaves approximately like a delta function and be represented as $\delta(x-x')$ When $x = x'$ the denominator goes to zero and hence the total quantity to ∞ When $x' \neq x$ then the function value is finite, ideally speaking it should be zero $x' \gg x$ or $x' \ll x$ the function becomes zero But such cases are not encountered due to finite dimensions of the specimen

Since conditions 1,2 and 3 are satisfied the four integral function reduces to $K'' M_0(x',y',z')$, where K'' is a constant With different x',y',z' the whole specimen can be imaged Simulation work carried out in Chapter 4 justifies this method The processing can be made real time, at least in theory with an array of chirp multipliers and integrators

CHAPTER 4

SIMULATION

4.1 STOCHASTIC NMR IMAGING SIMULATION

The excitation $H_1(t)$ can be realized with either a white sequence of pulses or continuous noise with zero mean. The particular distribution function is of no influence for evaluation of a linearly driven system. In particular a binary sequence of flip angles will be sufficient. Such sequences are easy to generate with feedback shift registers [15].

4.1.1 Discretization of the Spin Density

The second orthogonality condition is fulfilled by choosing distribution functions for the field gradients G_x, G_y, G_z with non zero mean.

In consideration of the third orthogonality condition it will be assumed for now that the measured response derives from a spin density, which, contrary to reality, is defined only on a discrete set of equidistant coordinate points x, y, z . This set of points shall be the same as the one on which the spin density $M_0(x', y', z')$ will be reconstructed by cross-correlation.

To avoid overlap of values, an interleaving set of discrete coordinates is constructed by setting

$$x' = (n_x + \alpha_x) a ,$$

$$y' = (n_y + \alpha_y) a ,$$

$$z' = (n_z + \alpha_z) a ,$$

where n_i is an integer, $0 < \alpha_i < 1$ for $i = x, y, z$ and the dimension of a discrete spin density element or picture cell is specified by 'a'. Similarly a discrete range of values is introduced for the gradient integrals

$$u = (n_u + \alpha_u) g$$

$$v = (n_v + \alpha_v) g$$

$$w = (n_w + \alpha_w) g$$

where n_i is an integer, $0 < \alpha_i < 1$ for $i = u, v, w$ and the product of the minimum field gradient step and the gradient switching interval Δt is denoted by g . Without loss of generality the field gradient switching interval will be assumed to be identical to the sampling interval, and hence the same symbol. The unit of g is rad/m. The value of g measures the minimum precession phase per picture cell which is acquired during one gradient step of length Δt . For a symmetrical distribution of gradient numbers n_i , the mean field gradients are $g_i = \alpha_i g / \Delta t$.

Evaluation of one of equations (3 11) provides insight into a choice for $\alpha_x, \alpha_y, \alpha_z$ and $\alpha_u, \alpha_v, \alpha_w$

$$x'u - y'v = [(n_x + \alpha_x)(n_u + \alpha_u) - (n_y + \alpha_y)(n_v + \alpha_v)] a g$$

The orthogonality condition states, that the right-hand side must be different from zero for all values of n_x, n_y, n_z and n_u, n_v, n_w . Setting $\alpha_x = \alpha_u, \alpha_y = \alpha_v, \alpha_z = \alpha_w$ it can be seen that

$$x'u - y'v = [n_x n_u + (n_x + n_u) \alpha_x + \alpha_x^2 - (n_y + n_v) \alpha_y - \alpha_y^2] a g$$

with

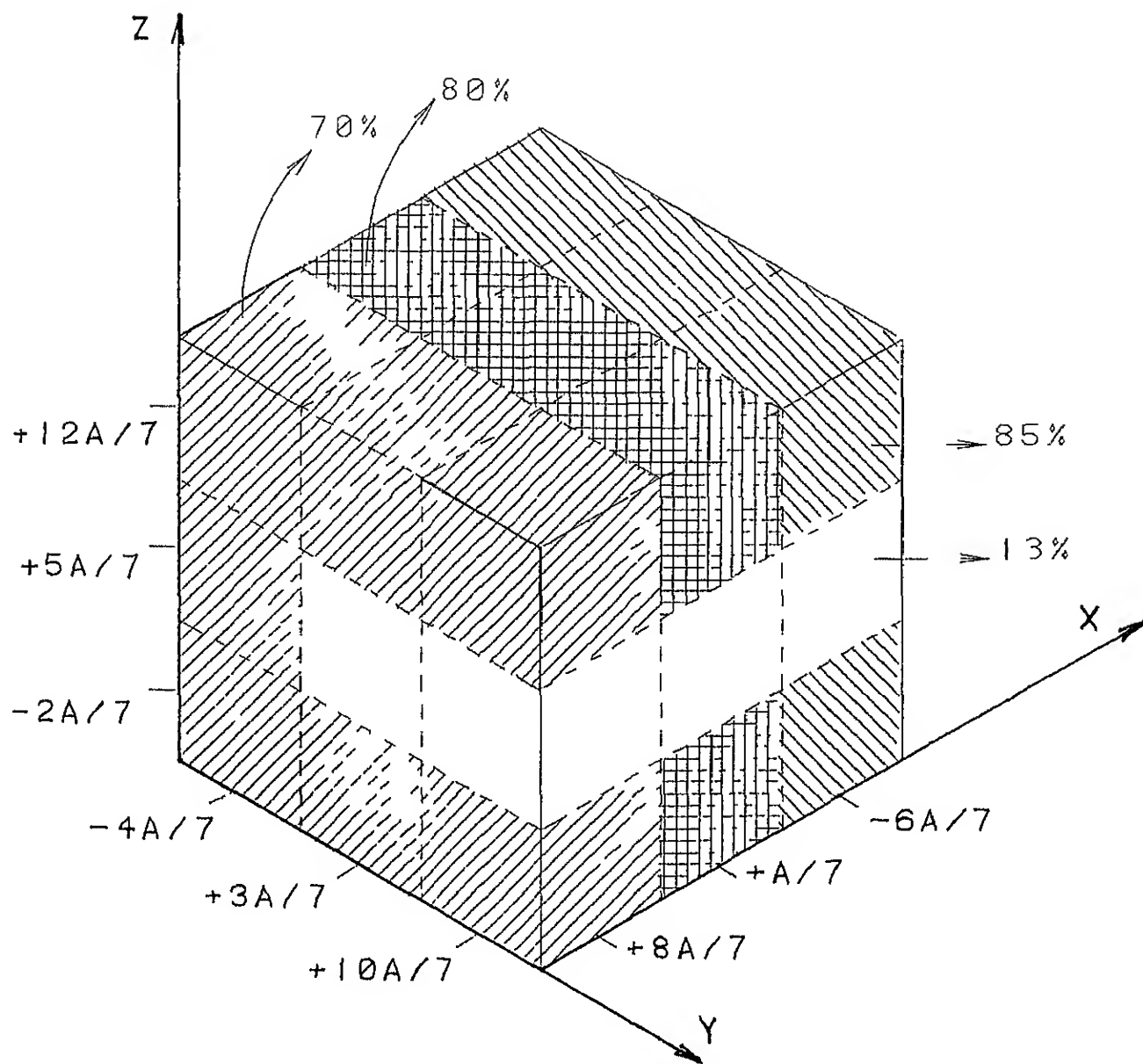
$$\begin{aligned} \alpha_x &= \alpha_u = 1/7, \\ \alpha_y &= \alpha_v = 3/7, \\ \alpha_z &= \alpha_w = 5/7 \end{aligned} \tag{4 1}$$

the third orthogonality condition is fulfilled by the interleaving coordinate and gradient integral values according to Eqs (3 10), (3 11), and (4 1)

4 1 2 Numerical Simulation

The linear response has been calculated according to Eqs (3 1), (3 10), and (4 1). The spin density was defined on a 3x3x3 mesh (Fig 4 1) with values reflecting proton densities of living tissues. The transverse relaxation time was $T_2 = 0.1$ sec. (As mentioned earlier this should be a

Fig 41 NMR 3-D SPIN DENSITY



spatial function, but here it is assumed to be constant) To keep the computation times at an acceptable level, the product of spatial resolution and precession was set to $\alpha\gamma = 2.5$ rad The sampling interval was 0.01 sec For each sampling interval new field gradient values and a new excitation value were derived from a 20 stage binary feedback shift register The excitation could assume two values, $H_1 = [-1/2, +1/2]$ with equal probability, while the field gradient numbers could assume four values, $n_x, n_y, n_z = [-3/2, -1/2, +1/2, +3/2]$ with probabilities 1/8, 3/8, 3/8, and 1/8 The field gradient numbers were obtained by shifting the feedback register thrice and adding the binary outputs of each shift

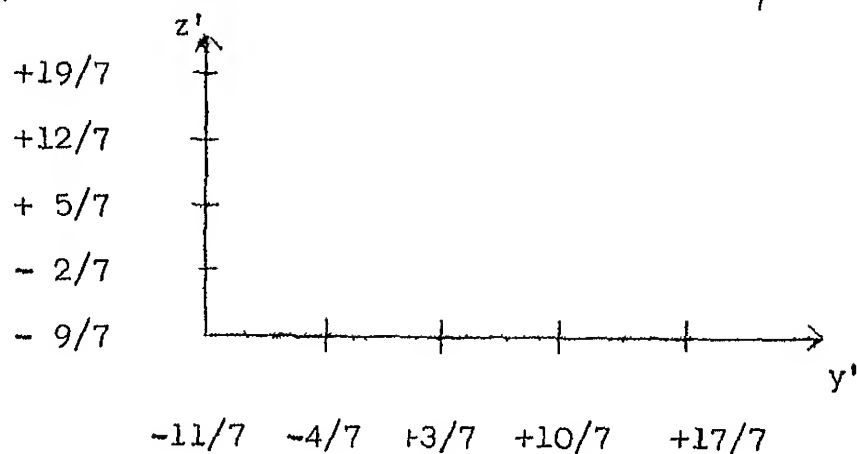
The cross-correlation was executed for a $5 \times 5 \times 5$ point mesh of the spin density $M_0(x', y', z')$ and a time shift $\sigma = T_2$ The result is shown in Fig. 4.2 in terms of slices showing $y'z'$ planes for different values of x' The numbers denote the retrieved spin density values percent The background noise results from the finite sample record length

For a random data ($0.0 \leq M_0(x, y, z) \leq 1.0$) also the simulation is carried out The assumed spin density and imaged values are shown in Fig. 4.3 All the spin densities shown in this chapter are percentile

3	3	2	-4	-1	-1	5	-7	1	-2
3	-1	9	-5	0	0	-2	7	0	-2
-12	7	4	-3	0	5	0	6	2	0
-6	-7	0	12	-1	-2	0	0	2	4
-1	1	-7	2	3	0	-2	7	0	-7

$$X' = -\frac{13}{7} a$$

$$X' = +\frac{15}{7} a$$



7	-11	4	6	0
-3	62	71	80	5
4	84	12	10	-5
9	77	73	77	-8
4	-3	-7	3	6

$$X' = +1/7 a$$

0	2	-6	-9	4	-5	4	5	-5	0
10	77	74	82	1	8	59	76	70	-2
-9	79	13	11	7	-17	73	12	12	-8
2	86	94	88	-6	4	69	62	77	-5
0	7	4	4	0	6	-5	0	0	5

$$X' = -\frac{6}{7} a$$

$$X' = +\frac{8}{7} a$$

Fig 4 2 Slices of retrieved spin density

$$X = -\frac{6}{7} a$$

19	32	6
73	10	71
60	18	63

$$X = +\frac{1}{7} a$$

4	37	40
67	53	79
39	88	43

$$X = +\frac{8}{7} a$$

1	39	36
13	29	13
67	18	68

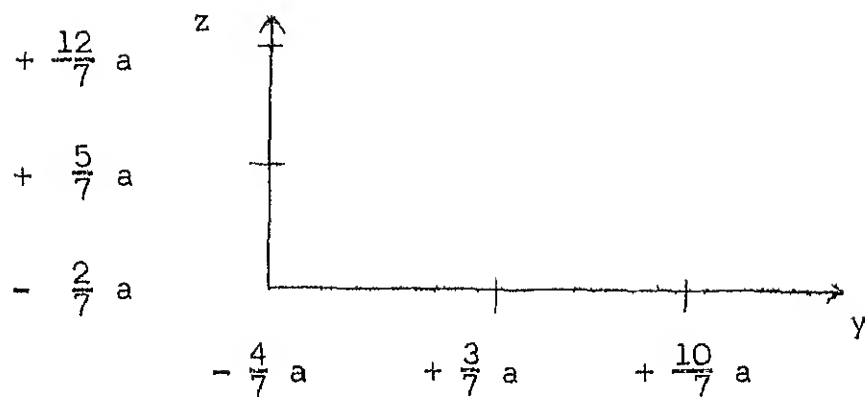
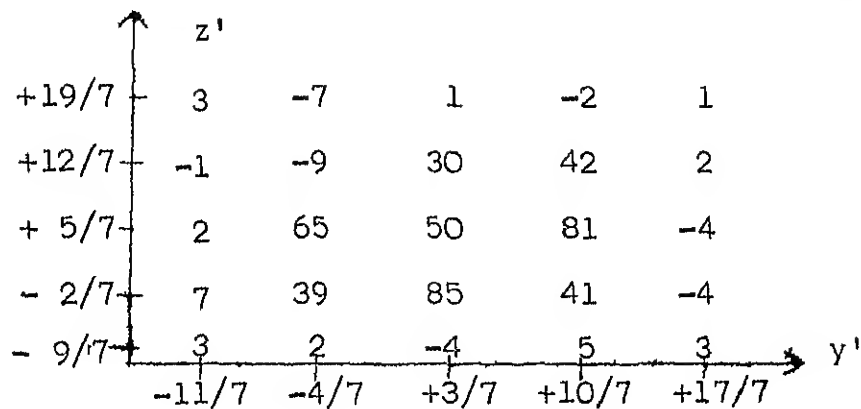


Fig 4 3(a) Spin density used in random simulation It is defined as a 3x3x3 array of cubic picture cells with dimension a

1	0	0	-4	-1	-7	3	-3	2	-1
3	-5	5	-3	0	0	1	9	-5	-5
-4	5	2	-6	0	0	4	5	-2	-1
-5	-6	-1	10	0	-3	0	0	0	1
-3	2	-5	0	3	3	0	8	0	-6

$$X' = -\frac{13}{7} a$$

$$X' = +\frac{15}{7} a$$



$$X' = +\frac{1}{7} a$$

1	0	-2	-2	0	-5	4	2	-6	-1
5	13	26	2	0	4	0	46	35	-1
-2	65	8	67	3	-7	16	26	12	-5
7	59	23	64	-3	1	67	7	72	-5
1	2	3	5	2	3	-5	0	0	2

$$X' = -\frac{6}{7} a$$

$$X' = +\frac{8}{7} a$$

Fig. 4 3(b) Retrieved Spin Density Slices

4.2 CHIRP IMAGING SIMULATION

Under this imaging scheme, we assume that $\pi/2$ pulse is applied and then FID signal is recorded in the presence of linear time function gradients. The pulse sequence is shown in Fig 4.4.

4.2.1 1-D Simulation

This process assumes that only a line of ^{volume} whole is excited and FID signal from other part is zero (Fig 4.5(b)). For one-dimension chirp imaging the FID signal can be written from Eq (3.12) as

$$y(t) = \int M_0(x) e^{jxK_1 t^2/2} dx$$

Here T_2 effect is not taken into consideration. When T_2 is assumed to be a constant its effect can be taken outside by multiplying $y(t)$ with e^{t/T_2} . 65536 samples of $y(t)$ are multiplied with $e^{-jx'K_1 t^2/2}$ and averaged over time to get $M_0(x')$ as shown below

$$\begin{aligned} & \int y(t) e^{-jx'K_1 t^2/2} dt \\ &= \int M_0(x) \int e^{jK_1(x-x') t^2/2} dt dx \\ &= \int M_0(x) d(x-x') dx \\ &= M_0(x') \end{aligned}$$

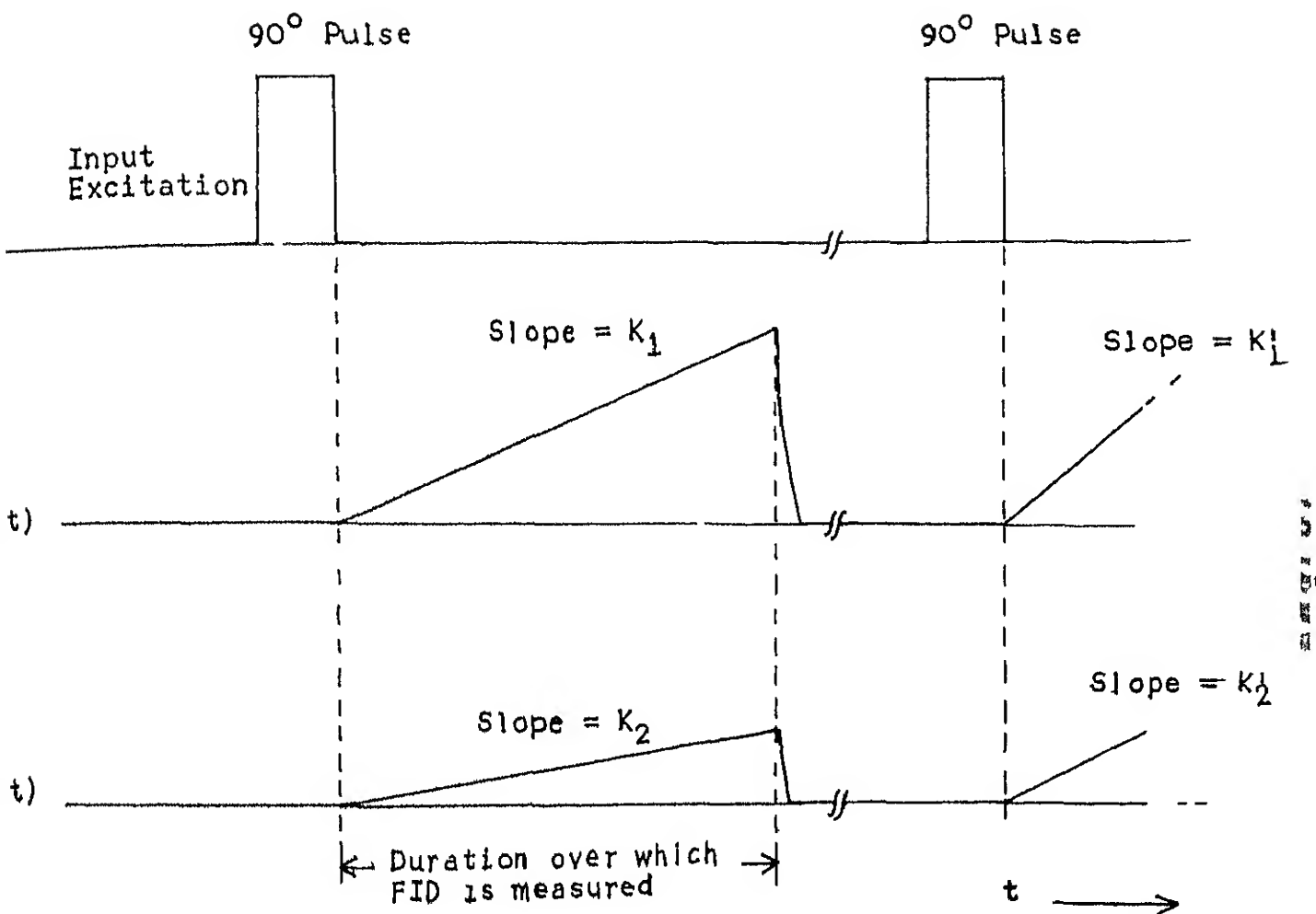


Fig 4.4 Pulse sequence for 2-dimensional chirp imaging

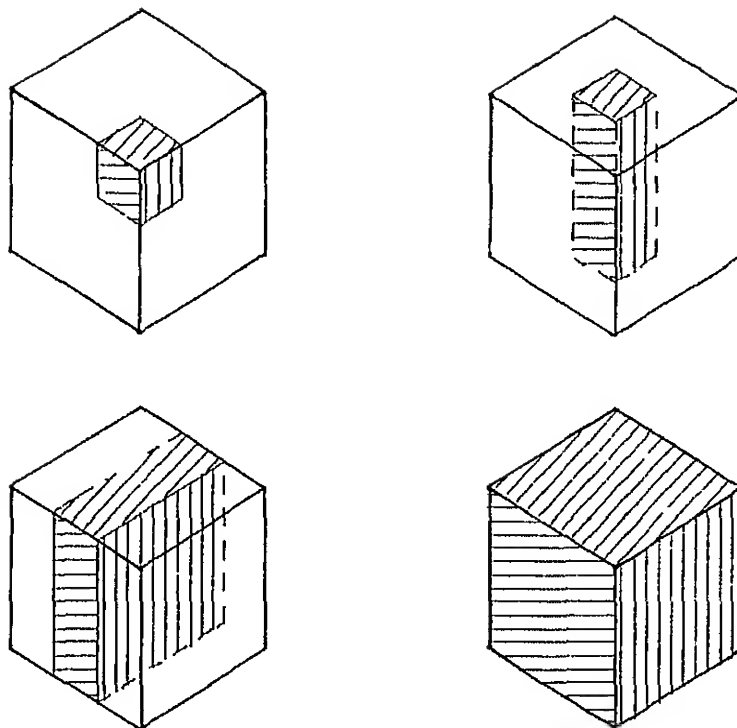


Fig 4.5

scheme of classification of imaging techniques (a) sequential point measurement (b) sequential line measurement, (c) sequential plane measurement, and (d) simultaneous volume measurement

For simulation, $M_0(x)$ is taken as

$M_0(1) = 19\%$, $M_0(2) = 73\%$, $M_0(3) = 60\%$, and imaged values are (using programs 5 and 6)

$M_0(1) = 25\%$, $M_0(2) = 77\%$, $M_0(3) = 64\%$ and $M_0(1) = 5.6\%$,

$M_0(4) = 6.6\%$

Ideal values of $M_0(-1)$ and $M_0(4)$ should be zero. These two values give idea of noise, where spin density is not present

4.2.2.2-D Simulation

This process assumes that only a slice of whole volume is excited [6], [20] and FID signal from remaining part is zero (Fig. 4.5(c)). For two-dimension chirp imaging the FID signal can be written from Eq. (3.12) as

$$y(t) = \iint M_0(x, y) e^{jK_1 x t^2/2} e^{jK_2 y t^2/2} dx dy$$

65536 samples of $y(t)$ are multiplied with $e^{-jK_1 x' t^2/2}$ and averaged over time to get $M(x', y')$ as given below

$$\begin{aligned} & \int y(t) e^{-jK_1 x' t^2/2} e^{-jK_2 y' t^2/2} dt \\ &= \iint M_0(x, y) \int e^{jK_1 (x-x') t^2/2} e^{jK_2 (y-y') t^2/2} dt dx dy \\ &= \iint M_0(x, y) \delta(x-x') \delta(y-y') dx dy \\ &= M_0(x', y') \end{aligned}$$

$M_0(x,y)$ is taken as slices (Fig 4 6) of spin density shown in Fig 4 1 The imaged values (Programs 7 and 8) are shown in Fig 4 7

Programs 7 and 8 are ran for random 2-D (slice) spin density Results are given in Fig 4 8 The first line in this slice is the same data ran for 1-D chirp imaging (Section 4 2 1) The imaged values for the first line are different from 1-D chirp imaged values which clearly indicates the correlation effect of two impulses, viz , $a(x-x')$ and $d(y-y')$

4 3 DETAILS OF PROGRAMS

The simulation work is carried out on DEC-1090 computer system Storage of 65536 complex values of FID signal requires about 2800 blocks The following gives details of programs The listings are given in Appendix

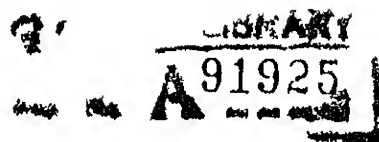
Program 1	Simulates stochastic magnetization - CPU time 6 hrs 5 mts 24 55 secs
Program 2	Cross-correlation for stochastic NMR tomography - 0 34 50 72
Program 3	Formatted printing of input
Program 4	Formatted printing of output
Program 5	Simulates 1-D chirp magnetization
Program 6	1-D chirp imaging
Program 7	Simulates 2-D magnetization - 0 2 53 12
Program 8	2-D chirp imaging -07 9 36

85	85	85	
85	13	13	Slice 1
85	85	85	
80	80	80	
80	13	13	Slice 2
80	80	80	
70	70	70	
70	13	13	Slice 3
70	13	13	

Fig 4 6 Slices of 3x3x3 spin density shown
in Fig 4 1

4	14	12	12	4	
4	96	93	93	4	
4	98	27	26	4	Slice 1
4	97	93	93	4	
4	14	12	12	4	-----
4	13	12	11	4	
4	91	88	87	4	
4	92	26	25	4	Slice 2
4	91	88	87	4	
4	14	12	11	4	-----
3	12	10	10	3	
3	79	77	76	3	
3	80	24	24	3	Slice 3
3	79	77	76	3	
3	12	10	10	3	

Fig 4 7 Imaged slices



19	73	60
32	10	18
6	71	63

Fig 4 8(a) 3x3 Input slice (spin density)
to Program 7

2	5	9	8	2
2	23	78	65	2
2	35	20	27	2
2	11	76	68	2
2	4	9	8	2

Fig 4 8(b) 5x5 Imaged slice through 2D
chirp imaging

CHAPTER 5

CONCLUSIONS

NMR techniques can be applied for imaging the protonic tissue matter in the whole body. The image can be obtained by a suitable set of gradient and RF signals and performing the appropriate signal processing. The image can be obtained point by point or line by line or slice by slice or total volume. Notable among the schemes are Fourier transform (FT) techniques and the correlation techniques. We have used PN sequence as the RF signal and spatially linear gradients as suggested by Blumich. The FID signal was simulated on the computer for a 3×3 matrix of 3 slices of spin density. The simulation of the FID signal took about 6 hours CPU time on DEC-1090 computer, and the processing on FID signal to recover the image about 30 minutes. Due to this large computer times involved larger matrix sizes, larger number of slices could not be tried out. A new scheme of obtaining the image through the chirp processing is implemented. In this scheme an RF signal is applied for a short duration followed by application of linear spatially and temporally varying gradient fields. The FID signal starting from the point of termination of RF signal is simulated, and the associated chirp processing is carried out.

The reconstructed images were found to be in good agreement with original spin density. The chirp method is applied for 1-D and 2-D imaging satisfactorily. But the results for 3-D were not encouraging.

For obtaining the NMR image of $3 \times 3 \times 3$ points from its FID signal approximately 1,769,472 complex multiplications and additions have to be performed by computer, which require a large computational time. The time required under the modalities involving FT techniques can be significantly cut down using Fast Fourier transform algorithms. However, chirp processing cannot be made faster due to lack of fast algorithms. It appears possible in any case to reduce the storage requirement and CPU time by using series-parallel processing, and should be attempted.

A detailed examination of the 3-D chirp is required to identify the reasons for unsatisfactory results we obtained. We have not applied any windows on the data to study their effects on side lobe levels. It appears possible to use appropriate window to improve the side lobe characteristics as done in conventional signal processing on finite data.

REFERENCES

- 1 Bloch F , 'Nuclear Induction', Physics Review, vol 70, pp 460-474, 1946
- 2 Blumich Bernhard, 'Stochastic NMR Imaging', Journal of Magnetic Resonance 60, pp 37-45, 1984
- 3 Blumich Bernhard and Spiess H W , 'NMR Imaging with Sinusoidal Field Gradient Modulation', Diskussionstagung der Fachgruppe Magnetische Resonanzspektroskopie der GDCh, 30 9-2 10 1985, Heidelberg
- 4 Blumich Bernhard, 'Stochastic NMR Spectroscopy', Bulletin of Magnetic Resonance, vol 7, No 1, pp 5-26
- 5 Blumich Bernhard and Spiess H W , 'NMR Imaging with Incommensurate Sampling and Gradient Modulation Rates', Journal of Magnetic Resonance, January 1986
- 6 Caprihan Arving, 'Effect of Amplitude Modulation on Selective Excitation in NMR Imaging', IEEE Transactions on Medical Imaging, vol MI-2, No 4, pp 169-175, December 1983
- 7 Cho Z H , Kim H S , Song H B , and James Cumming, 'Fourier Transform Nuclear Magnetic Resonance Tomographic Imaging', Proceedings of the IEL, vol 70, No 10, pp 1152-1173, October 1982
- 8 Damadian Raymond, 'Tumor Detection by NMR', Science, vol 171, No 3976, pp 1151-1153, 19 March 1971

- 9 Feiner L F and Locher P P , 'On NMR Spin Imaging by Magnetic Field Modulation', Applied Physics 22, pp 257-271, 1980
- 10 Derusso P M , Roy R J , and Close C M , State Variables for Engineers, John Wiley and Sons, Inc , 1967
- 11 Hinshaw Waldo S , and Lent Arnold H , 'An Introduction to NMR Imaging From the Bloch Equation to the Imaging Equation', Proceedings of the IEEE, vol 71, No 3, pp 338-350, March 1983
- 12 Hoult D I , 'The Solution of the Bloch Equations in the Presence of a Varying B_1 Field - An Approach to Selective Pulse Analysis', Journal of Magnetic Resonance 35, pp 69-86, 1979
- 13 House Waylon V , 'Introduction to the Principles of NMR', IEEE Transactions on Nuclear Science, vol NS-27, No 3, pp 1220-1226, June 1980
- 14 Klauder J R , Price A C , Darlington S , and Albersheim W J , 'The Theory and Design of Chirp Radars', The Bell System Technical Journal, vol 39, No 4, pp 745-808, July 1960
- 15 Korn C.A , Random Process, Simulation and Measurement, McGraw-Hill, New York, 1966
- 16 Lauterbur P C , 'Image Formation by Induced Local Interactions Examples Employing Nuclear Magnetic Resonance', Nature, vol 242, pp 190-191, March 16, 1973

- 17 Locher P R , 'Computer Simulation of Selective Excitation in NMR Imaging', Philosophical Transactions of Royal Society of London, B 289, pp 537-542, 1980
- 18 Mansfield P and Morris P G , 'NMR Imaging in Biomedicine', Supplement 2, in advances in Magnetic Resonance, 'Laugh J S , Ed New York Academic, 1982
- 19 Schwarz Ralph J and Friedland Bernard, Linear Systems, McGraw-Hill Book Company, 1965
- 20 Smith M R , 'RF Pulse Shapes for Selective Excitation in NMR Imaging', IEEE Transactions on Medical Imaging, vol MI-4, No 2, pp 79-83, June 1985

i

SP.4 DENSITY CONTRAST: 85%, 80%, 70%, 13%

```

      DO 101 J=1,3
      DO 101 K=1,3
101   RO(1,J,K)=0.85
      DO 102 J=1,3
      DO 102 K=1,3
102   RO(2,J,K)=0.80
      DO 103 J=1,3
      DO 103 K=1,3
103   RO(3,J,K)=0.70
      DO 110 I=1,3
      DO 110 J=2,3
110   RO(1,J,2)=0.13
      END
*
      SUBROUTINE MAGN
*
      COMMON/PHSE/ISROLL
      COMMON/PARM/RO(3,3,3),ITAU,S,R,IPRES,IEND
      COMMON/SHIFT/GRX(50),GRY(50),GRZ(50),IEX(50),IREG(21),EOR
      COMMON/CONST/CX,CY,CZ,FX,FY,FZ,AG
      INTEGER IREG,EOR,IEX,IRAN,GRX,GRY,GRZ
      COMPLEX S,R
*
      CONVOLUTION INTEGRAL
      CALL PRESNT
      N=0
      DO 400 ITAU=1,IEND
      IO=ISROLL+1-ITAU
      IF(IO.GE.0) IO=50+IO
      SPACE INTEGRALS
      FTIME=(1.-ITAU)/10.
      S=0.
      IX=GRX(IO)+CX
      IY=GRY(IO)+CY
      IZ=GRZ(IO)+CZ
      DO 300 IX=1,3
      DO 300 IY=1,3
      DO 300 IZ=1,3
      S=(IX-FX)*GX+(IY-FY)*GY+(IZ-FZ)*GZ
100   S=S+RO(IX,IY,IZ)*CEXP(COMPLEX(FTIME,0*AG))
      CONVOLUTION INTEGRAL
      REX=S+IEX(IO)
      END
*
      SUBROUTINE PRESNT
*
      COMMON/PHSE/ISROLL
      COMMON/PARM/RO(3,3,3),ITAU,S,R,IPRES,IEND
      COMMON/SHIFT/GRX(50),GRY(50),GRZ(50),IEX(50),IREG(21),EOR
      COMMON/CONST/CX,CY,CZ,FX,FY,FZ,AG
      INTEGER IEX,IGY,IGZ ARE DOUBLE PRECISION
      INTEGER IREG,EOR,IEX,IRAN,GRX,GRY,GRZ,IGX,IGY,IGZ
      COMPLEX S,R
      GRADIENTS
      IPRES=IPRES+1
      ISROLL=ISROLL+1
      IF(ISROLL.GT.50) ISROLL=1
      IEX=IRAN(1)
      IGY=IRAN(2)
      IGZ=IRAN(3)
      GRX(ISROLL)=IGX
      GRY(ISROLL)=IGY
      GRZ(ISROLL)=IGZ
      CELESTATION
      IEX(ISROLL)=IRAN(1)
      DO 400 GRADIENT INTEGRAL TABLE
      IEND=50
      IF(IPRES.GT.IEND) IEND=IPRES
      IEND=I
      DO 400 J=1,3
      DO 400 K=1,3

```

```

DD 300  ITAU=1,J
IO=ISROLL-ITAU
IF(10.LE.0) IO=50+IO
GRX(10)=GRX(10)+IGA
GRY(10)=GRY(10)+IGY
GRZ(10)=GRZ(10)+IGZ
END

```

```

FUNCTION IRAN(K)

```

```

COMMON/PHSE/ISROLL
COMMON/PARM/RO(3,3,3),ITAU,S,R,IPRES,IEND
COMMON/SHIFT/GRX(50),GRY(50),GRZ(50),IEX(50),IREG(21),EOR
COMMON/CONST/CX,CY,CZ,FX,FY,FZ,AG
INTEGER IREG,EOR,IEX,IRAN,GRX,GRY,GRZ
COMPLEX S,R

```

```

IRAN=0
DD 200  J=1,K
DD 100  I=1,20
IREG(22-I)=IREG(21-I)
EOR=IREG(21)+IREG(18)
IREG(1)=EOR-2*(EOR/2)
IRAN=IRAN+IREG(20)
IRAN=2.*(IRAN-K/2.)
END

```

PROGRAM 2

THIS PROGRAM PERFORMS CROSS-CORRELATION FOR STOCHASTIC NMR TOMOGRAPHY

SUMMARY:

This program reads the sampled values of FID(RES(1) to RES(65536)) generated by program 1. This program generates same input excitation and field gradient values to reconstruct the Spin Density. These values are generated in a sequence from a RAM (random) subprogram to avoid dimension declaration in order to save space. The theory of this program is discussed in chapter 4. The Spin Density coordinates are decided by CX, CY, CZ and FX, FY, FZ. The reconstructed Spin Density is a 3-Dimension function. The input to this program is the output of program 1. This program requires about 30 minutes CPU time. The output is a 5X5X5 matrix. Comparison with the 3X3X3 input gives the idea of deviation error (comparing same points) and truncation error and noise (comparing the points for which Spin Density values are not assigned). Same cell width value (AG=2.5) is to be used. The assumed delay(SIGMA) is 0.1 sec.

```
.....
COMMON/PHSE/ISROLL
COMMON/PARM/RO(5,5,5),RESP(64),IPRES,IEND
COMMON/SHIFT/GRX(50),GRY(50),GRZ(50),LEX(50),IREG(21),EOR
COMMON/CONST/CX,CY,CZ,FX,FY,FZ,AG,ISIGMA
INTEGER IREG,EOR,LEX,IRAN,GRX,GRY,GRZ
```

```
COMPLEX RESP
MAIN PROGRAM
CALL INITIA
DO 500 I=1,1023
  READ(21,*) (RESP(J),J=1,64)
  CALL SMOBS
  F=(EXP((ISIGMA-1.)/10.))/(64.*1024.)
  DO 500 J=1,5
    DO 500 K=1,5
      RO(I,J,K)=RO(I,J,K)*F
      IREG(22,*)=(RO(I,J,K),K=1,5)
    STOP
  END
```

SUBROUTINE INITIA

```
COMMON/PHSE/ISROLL
COMMON/PARM/RO(5,5,5),RESP(64),IPRES,IEND
COMMON/SHIFT/GRX(50),GRY(50),GRZ(50),LEX(50),IREG(21),EOR
COMMON/CONST/CX,CY,CZ,FX,FY,FZ,AG,ISIGMA
INTEGER IREG,EOR,LEX,IRAN,GRX,GRY,GRZ
```

```
COMPLEX RESP
CALL WIDTH IN RAD/2
```

```
AG=2.5/2.
DELAY SIGMA: T2=10
```

```
ISIGMA=40
IMPLICIT COMPLEX
```

```
CM=1./7.
CY=1./7.
CZ=5./7.
```

```
FX=3.-3X
FY=3.-3Y
FZ=3.-3Z
```

```
SHIFT REGISTER
DO 10 I=1,21
```

```
IREG(I)=1
DO 10 K=1,5
```

```
IRAN=50
IPRES=50
```

```
IPRES=50
```

```

*      SOIL DENSITY
DO 2, I=1,5
DO 2, J=1,5
DO 2, K=1,5
30(I,J,K)=0.
*      START=00 PHASE
READ(21,*) (RESP(J), J=1,64)
DO 100 J=1,64
CALL PRESNT
END

*      SUBROUTINE CROSS
*
COMMON/PHSE/ISROLL
COMMON/PARM/RO(5,5,5),RESP(64),IPRES,IEND
COMMON/SHIFT/GRX(50),GRY(50),GRZ(50),IEX(50),IREG(21),EOR
COMMON/CONST/CX,CY,CZ,FX,FY,FZ,AG,ISIGMA
INTEGER IREG,EOR,IEX,IRAN,GRX,GRY,GRZ
*      NOTE: AM IS COMPLEX
*      COMPLEX RESP,AM
*      CROSS CORRELATION
DO 300 I=1,64
CALL PRESNT
IO=ISROLL+I-ISIGMA
IF(IO.GE.0) IO=50+IO
AM=RESP(I)+IEX(IO)
IX=GRX(IO)+CX
IY=GRY(IO)+CY
IZ=GRZ(IO)+CZ
DO 300 IX=1,5
DO 300 IY=1,5
DO 300 IZ=1,5
O=(IX-FX)*IGX+(IY-FY)*IGY+(IZ-FZ)*IGZ
RO(IX,IY,IZ)=RO(IX,IY,IZ)+AM*CEXP(CMPLX(0.,-D*AG))
END

*      SUBROUTINE PRESNT
*
COMMON/PHSE/ISROLL
COMMON/PARM/RO(5,5,5),RESP(64),IPRES,IEND
COMMON/SHIFT/GRX(50),GRY(50),GRZ(50),IEX(50),IREG(21),EOR
COMMON/CONST/CX,CY,CZ,FX,FY,FZ,AG,ISIGMA
*      NOTE: IGX,IGY,IGZ ARE DOUBLE PRECISION
INTEGER IREG,EOR,IEX,IRAN,GRX,GRY,GRZ
*      COMPLEX RESP
*      GRADIENTS
IPRES=IPRES+1
ISROLL=ISROLL+1
IF(ISROLL.GT.50) ISROLL=1
IGX=IRAN(3)
IGY=IRAN(4)
IGZ=IRAN(5)
GRA(ISROLL)=IGX
GRY(ISROLL)=IGY
GRZ(ISROLL)=IGZ
*      EXITATION
IEX(ISROLL)=IRAN(1)
*      UPDATE GRADIENT INTEGRAL VALUE
IEND=ISIGMA
IF(IPRES.GT.IEND) IEND=IPRES
I=IEND-1
IF(I.GE.0) GO TO 400
DO J=1,64
DO I=1,64
DO K=1,64
IO=ISROLL+I-ISIGMA
IF(IO.GE.0) IO=50+IO
IX=GRX(IO)+CX
IY=GRY(IO)+CY
IZ=GRZ(IO)+CZ

```

END

FUNCTION IRAN(K)

COMMON/PHSE/ISROLL

COMMON/PARM/RO(S,5,5),RESP(64),IPRES,IEND

COMMON/SHIFT/GRX(50),GRY(50),GRZ(50),IEX(50),IREG(21),EOR

COMMON/CONST/CX,CY,CZ,FX,FY,FZ,AG,ISIGMA

INTEGER IREG,EOR,IEX,IRAN,GRX,GRY,GRZ

COMPLEX RESP

IRAN=0

DO 200 J=1,K

DO 100 I=1,20

IREG(22-I)=IREG(21-I)

EOR=IREG(21)+IREG(18)

IREG(1)=EOR-2*(EOR/2)

IRAN=IRAN+IREG(20)

IRAN=2.*(IRAN-K/2.)

END

```

*****
*      PROGRAM 3      *
*****
* THIS PROGRAM PRINTS THE RANDOM 3-D INPUT SPIN DENSITY IN 3(3X3) MATRICES
* .....
  DIMENSION RD(5,5,5)
  DO 101 I=1,3
  DO 101 J=1,3
  DO 101 K=1,3
    R12=BRAN(34)
    R22=R12*100
    I111=R22
  101 RD(I,J,K)=I111
  DO 102 I=1,3
  WRITE(20,99)
  99  FORMAT(///)
  DO 102 J=1,3
  102 WRITE(20,100)(RD(I,J,K),K=1,3)
  100  FORMAT(' ',3(' ',F4.1)/)
  STOP
  END

```



```

*****
PROGRAM 5
*****
THIS PROGRAM GENERATES 65536 SAMPLE POINTS
(FID SIGNAL) OF 1-D CHIRP IMAGING.
The theory of this program is discussed in chapter 4 in 1-D
Chirp Imaging. The Spin Density is considered to be 1 dimension.
The sampled values of FID are given sequentially from 1 to
65536.
.....
COMPLEX S
DIMENSION RO(3)
OPEN (UNIT=21, FILE='FOR21.DAT', DEVICE='DSKD')

FOLLOWING INITIALIZES SPIN-DENSITY AND CX, FX, AG etc.
AG=2.5/2.
OFF SET CONSTANTS
CX=1./7.
FX=2.-CX
G: CHIRP RATE DENOTED AS K/2 IN THE ANALYSIS
G=10.
THRO: RAN FUNCTION 1-D RANDOM SPIN DENSITY IIS GENERATED HERE.
DO 101 IS=1,3
R12=RAN(1)
R22=R12*100
I111=R22
RO(IS)=I111/100.0
101 CONTINUE

FID AT VARIOUS POINTS SAMPLED

DO 200 IP=1, 65536
IP=IP*G/65536.
TIME=-T/0.1
CX=EXP
S=0.
DO 300 IX=1,3
D=(CX-FX)*GX
S=S*RO(IX)*CEXP(CMPLX(0.,D*AG))
300 CONTINUE
WRITE(21,*)S
200 CONTINUE
STOP
END

```

```

*****
* PROGRAM 5 *
*****
* THIS PROGRAM PERFORMS INVERSE CHIRP PROCESSING (1-D IMAGING)*
* FOR PROGRAM 5(1-D CHIRP PROCESSING)
* The input to this program is the output of program 5.
*.....
* DIMENSION RO(5)
* COMPLEX FUN
* CELL WIDTH IN RAD/2
* AG=2.5/2.
* OFFSET CONSTANTS
* CX=1./7.
* FX=3.-CX
* G: CHIRP RATE, DENOTED AS K/2 IN ANALYSIS.
* G=10.
* DO 20 I=1,5
20 RO(I)=0.
*
* DO 40 IT=1,65536
* READ(21,*)FUN
* I=IT*G/65536.
* CX=T*T
* DO 30 IX=1,5
30 U=(IX-FX)*GX
40 RO(IX)=RO(IX)+FUN*CEXP(CMPLX(0.,-0*AG))
* CONTINUE
* F=1./(54.*1024.)
* DO 50 I=1,5
50 RO(I)=RO(I)*F
* WRITE(22,*)RO(I)
* STOP
* END

```

```

*****
* PROGRAM 7
*****
* THIS PROGRAM GENERATES 65536 SAMPLE VALUES
* (OF FID SIGNAL) OF 2-D CHIRP PROCESSING.
* FOLLOWING INITIALIZES SPIN-DENSITY AND CX,FX,AG etc.
*.....
COMPLEX S,RESP
DIMENSION RO(5,5),RESP(64),R(29)
OPEN (UNIT=21,FILE='FOR21.DAT',DEVICE='DSKD')

* CELL WIDTH IN RAD/2
AG=2.5/2.
* OFFSET CONSTANTS
CX=1./7.
CY=3./7.
FX=2.-CX
FY=2.-CY
* G1,G2 ARE CHIRP RATES DENOTED AS HALF OF K1,K2 RESPECTIVELY IN ANALYSIS
G1=9.123456789
G2=57.098765430

IT=0
K=0
DO 10 IS=1,5
DO 10 JS=1,5
K=K+1
THIS PROGRAM GENERATES SPIN DENSITY SLICE VALUES RANDOMLY.
FOR EXECUTION THIS PROGRAM HAS TO BE LINKED WITH INSL.
CALL GSUB(192,25,R)
R12=R(K)
R22=R12*100
I111=R22
RO(IS,JS)=I111/100.0
CONTINUE

FID AT VARIOUS POINTS SAMPLED
DO 30 I=1,1024
DO 40 J=1,64
IT=I+1
GX=(IT*G1/65536.)*2
GY=(IT*G2/65536.)*2
S=0.
DO 20 IX=1,5
DO 20 IY=1,5
S=(IX*FX)+GX+(IY*FY)+GY
S=S*RO(IX,IY)*CEXP(CMPLX(0.,D*AG))
RESP(J)=S
WRITE(21,*)(RESP(J),J=1,64)
STOP
END

```

```

*****
PROGRAM 8
*****
THIS PROGRAM PERFORMS INVERSE 2-D CHIRP PROCESSING (2-D IMAGING)
FOR PROGRAM 7(2-D CHIRP PROCESSING)
.....
DIMENSION RO(7,7),FUN(64)
COMPLEX FUN
CELL WIDTH IN RAD/2
AG=2.5/2.
OFFSET CONSTANTS
CX=1./7.
CY=3./7.
KX=3.-CX
KY=3.-CY
G1,G2: CHIRP RATES DENOTED AS HALF OF K1,K2 IN ANALYSIS.
G1=9.123456789
G2=57.998765430
IT=0

DO 10 I=1,7
DO 10 J=1,7
RO(I,J)=0.

DO 40 I=1,1024
READ(21,*) (FUN(J),J=1,64)
DO 30 J=1,64
IT=IT+1
GX=(IT*G1/55536.)*2
GY=(IT*G2/55536.)*2
DO 20 IX=1,7
DO 20 IY=1,7
S=(IX-CX)*GX+(IY-CY)*GY
RO(IX,IY)=RO(IX,IY)+FUN(J)*2*EXP(CMPLX(0.,-D*AG))
CONTINUE
F=1./64.*1024.
DO 50 I=1,7
DO 50 J=1,7
RO(I,J)=RO(I,J)*F
WRITE(22,*) RO(I,J)
STOP
END

```

A 91925

EE-1986-M-KUM-SYS